Rare Metal Materials and Engineering
Volume 46, Issue 12, December 2017
Online English edition of the Chinese language journal

Available online at www.sciencedirect.com
ScienceDirect

Cite this article as: Rare Metal Materials and Engineering, 2017, 46(12): 3669-3674.

ARTICLE

Synthesis of Ag/AgCl Nanoparticles Immobilized on $CoFe_2O_4$ Fibers and Their Photocatalytic Degradation for Methyl Orange

Li Ziyu, Jia Zhigang, Li Wenwen, Liu Jianhong, Jiang Shan, Li Shengbiao, Zhu Rongsun

Anhui University of Technology, Ma'anshan 243002, China

Abstract: Ag/AgCl nanoparticles were immobilized onto the as-prepared $CoFe_2O_4$ fibers by a facile synthesis method. The amount of Ag/AgCl nanoparticles immobilized onto $CoFe_2O_4$ fibers could be tuned. The as-synthesized Ag/AgCl@$CoFe_2O_4$ composite fibers were characterized by XRD, FESEM and EM, and employed to degradate MO (methyl orange) dye in wastewater under visible light. The results show that AAC-4 fiber exhibits higher efficiency for the degradation of the MO dye under visible light illumination than other Ag/AgCl@$CoFe_2O_4$ composite fibers or pure Ag/AgCl sample, and the decolorizing efficiency of MO can research 98.2%. The immobilization of Ag/AgCl nanoparticles onto $CoFe_2O_4$ fiber promotes the enhancement of photocatalytic efficiency and stability.

Key words: immobilization; photocatalytic activity; methyl orange; degradation

With the development of modern industry, water pollution caused by the organic dyes poses severe challenges to the ecosystem and human health due to the organic dyes of toxicity and non-biodegradability[1]. In the past several years, many efforts have been done to find simple and effective methods to eliminate dye pollutant from wastewater. Traditional chemical and biological-based processes are used for wastewater treatment but have several disadvantages[2-4].

Light photocatalytic degradation has attracted considerable attention to solve the aromatically structured organic dyes because of potential improvements in simplicity and cost-effectiveness[5]. The irradiation of photocatalytic semiconductor materials with specific wavelength of light results in the formation of electron-hole couples which promote reduction and oxidation reactions. This unique property of semiconductors has been used to develop environmental remediation technologies for wastewater treatment[6-8].

In the various semiconductors, titanium dioxide (TiO_2) is a sufficient available and non-toxic semiconductor. The photocatalyst design based on TiO_2 was widely investigated. However, the large band gap and low electron-hole separation efficiency of TiO_2 in visible light spectra restrict its application[9]. Silver/silver halide (Ag/Ag*X*) possesses high efficiency for visible light utilization because of the surface plasmon resonance of metallic Ag and its synergistic effect with the photosensitive characteristic of Ag*X*. Among the various plasmonic photocatalysts, Ag/AgCl-based composites have received considerable attention owing to the outstanding photocatalytic performance and excellent stability[10].

However, it is difficult to recover ultrafine Ag/AgCl powder from the aqueous dispersion after the photodegradation process. Immobilization of Ag/AgCl particles on substrates is an effective method to resolve

Received date: December 25, 2016
Foundation item: National Natural Science Foundation of China (20907001); Training Programs of Innovation for Undergraduates of Anhui University of Technology (2015019)
Corresponding author: Jia Zhigang, Ph. D., Professor, School of Chemistry and Chemical Engineering, Anhui University of Technology, Ma'anshan 243002, P. R. China, Tel: 0086-555-2311807, E-mail: zjchemyue@126.com

these problems[11]. The application of magnetic carrier in environmental field is one of several new and innovative methods that have received considerable attention in recent years[12-14]. Compared with conventional separation, the advantages of magnetic carrier come from its speed, accuracy, and simplicity. Magnetic particles can be used as carrier for various active materials and the active materials can be randomly separated from the solution by a simple magnetic process. In the present work, Ag/AgCl nanoparticles were immobilized onto $CoFe_2O_4$ fibers and their photocatalysis degradation for MO was investigated in detail.

1 Experiment

Silver nitrate, cobalt sulfate heptahydrate, iron (II) sulfate heptahydrate, oxalic acid, methyl orange (MO) and sodium chloride were of analytical grade and used as received. Deionized water was used as the solvent for all of the solutions or dispersions.

$CoFe_2O_4$ fibers were used as carrier of activated photocatalytic materials. $CoFe_2O_4$ fibers were firstly synthesized according to our previous reports[15]. Typically, 2 mmol $CoSO_4 \cdot 7H_2O$ and 4 mmol $FeSO_4 \cdot 7H_2O$ were dissolved into 80 mL ethylene glycol (EG)/water (W) solvent with the volume ratio of V_{EG}/V_W=3:1. Then, 6 mmol $H_2C_2O_4 \cdot 2H_2O$ were added into the above-mentioned solvent. Subsequently, the mixture was transferred to a 100 mL Teflon-lined stainless steel autoclave and kept at 120 ℃ for 10 h. After cooling to room temperature, the final products were collected by washing with deionized water and three times with ethanol, and then dried at 100 ℃. The obtained product was calcined at 500 ℃ for 2 h to obtain $CoFe_2O_4$ fibers.

The as-prepared $CoFe_2O_4$ fibers were employed as carrier of nanosized Ag/AgCl composite. The specific synthesis process can be described as follows: 50 mg $CoFe_2O_4$ fibers were added into 50 mL PVP solution (40 wt%). Then, $CoFe_2O_4$ fibers were separated by a magnet, washed several times and redispersed into 40 mL $AgNO_3$ solution. NaCl solution (40 mL) with the same concentration was added into $AgNO_3$ solution drop by drop under vigorous stirring in 40 min. After the addition was finished, the mixture was exposed to 125 W UV light with the distance of 15 cm for 10 min. Finally, the sample was magnetically separated from the solution and dried for the further use. The concentration of solution was set as 1.25, 2.5, 5 and 7.5 mmol/L, respectively. Accordingly, the as-prepared samples were named AAC-1, AAC-2, AAC-3 and AAC-4, respectively. Pure Ag/AgCl sample and $CoFe_2O_4$ fibers named as AAC-0 were also prepared.

The phase purity and crystal structure of the obtained samples were examined by X-ray diffraction (XRD, Bruker D8 Advance X-ray diffractometer) with Cu-Kα radiation (λ=0.154 06 nm). The morphologies of the resulting samples were characterized by a field emission scanning electron microscopy (Nova NanoSEM 450, Holland) and electron microscope (LI00 S600T, Germany).

The photocatalytic activities of AAC composites were evaluated with the catalytic degradation of MO under irradiation using a 500 W xenon lamp equipped with a 400 nm cut-off filter. For each test, 0.05 g catalyst powder was added into 100 mL 10 mg/L MO solution. The test solutions were stirred in the dark for 30 min before irradiated under the visible light. During the irradiation, 3 mL sample of the reaction suspension was taken every 3 min. The supernatant was collected and analyzed on the visible spectrophotometer. Photocatalytic degradations of MO in the dark in the presence of the photocatalyst and under visible light irradiation in the absence of the photocatalyst were also used as negative controls.

2 Results and Discussion

The phase composition of the magnetic carrier, typical carrier modified by AgCl and AAC-4 photocatalyst was determined with XRD as shown in Fig.1. The diffraction peaks of $CoFe_2O_4$ corresponding to 2θ values of 30.10°, 35.72°, 42.98°, 56.79°, and 62.41° are confirmed as the planes (220), (311), (400), (511), and (440), respectively. The pattern can be identified as spinel $CoFe_2O_4$ with the lattice parameters of a cubic structure (space group Fd3m, JCPDS card No. 82-1049). The peaks of AgCl@$CoFe_2O_4$ at 2θ=27.8°, 32.2°, 46.2°, 54.8° and 57.5° are attributed to (111), (200), (220), (311) and (222) crystal planes of AgCl (JCPDS No. 85-1355) besides the characterization peaks of $CoFe_2O_4$, indicating the formation of AgCl@$CoFe_2O_4$ composite. The peaks of Ag/AgCl@$CoFe_2O_4$ at 2θ=38.1° can be ascribed to the metallic Ag (JCPDS No. 87-717) and the weak peak intensity can be ascribed to the minor deposition amount under light illumination[16]. No characteristic peaks attributing to impurities or other phases are detected besides the characterization peaks of $CoFe_2O_4$ and AgCl, demonstrating that the obtained product is composed of metallic Ag, AgCl and $CoFe_2O_4$ phase.

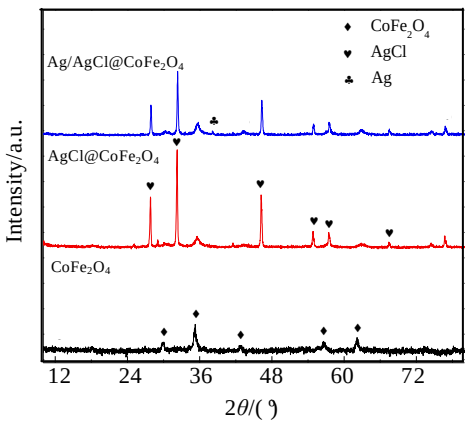

Fig.1 XRD patterns of the as-prepared samples

SEM and EM images of AAC-0 ($CoFe_2O_4$ fiber) and AAC-4 fibers are illustrated in Fig.2. The as-prepared $CoFe_2O_4$ carrier is fiber-like morphology with high aspect ratio as shown in Fig.2a. Fig.2b is the SEM image of AAC-4 sample. It is easy to observe that plenty of nanoparticles adhere to the surface of $CoFe_2O_4$ carrier. The change can also be found through the EM images of $CoFe_2O_4$ fiber and AAC-4 sample as shown in Fig.2c and 2d. The surface of AAC-4 sample becomes rough while the surface of $CoFe_2O_4$ fiber is relatively smooth because of the attachment of Ag/AgCl nanoparticles.

The formation process of Ag/AgCl@$CoFe_2O_4$ fiber can be illustrated in Fig.3. The surface of $CoFe_2O_4$ fiber is firstly coated with PVP molecules. Ag^+ and PVP chains form a Ag^+-PVP complex in liquid solutions, and the Ag^+ ions uniformly disperse in the voids of PVP chains[17].

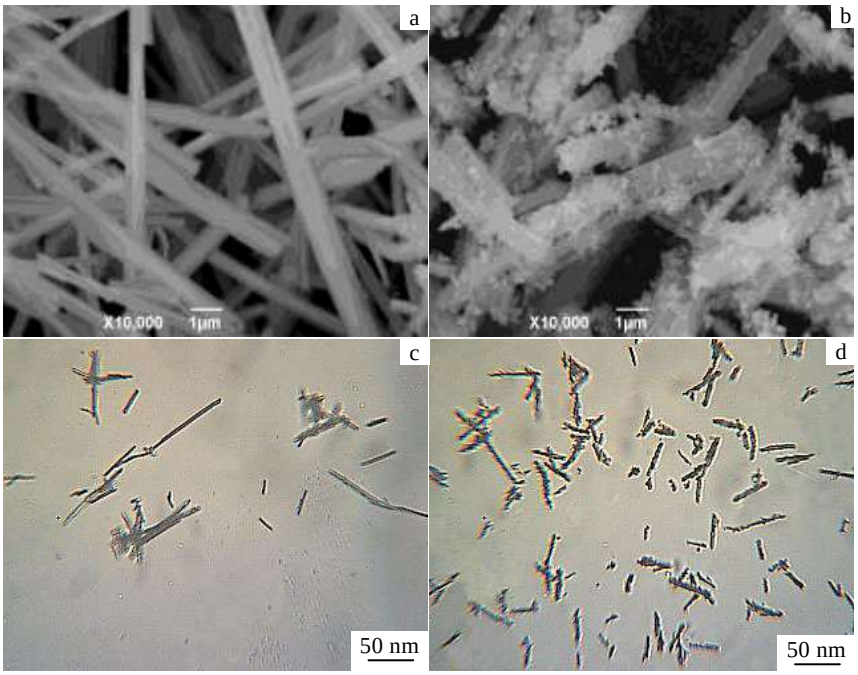

Fig.2 SEM (a, b) and EM (c, d) images of $CoFe_2O_4$ (AAC-0) (a, c) and Ag/AgCl@$CoFe_2O_4$ (AAC-4) (b, d)

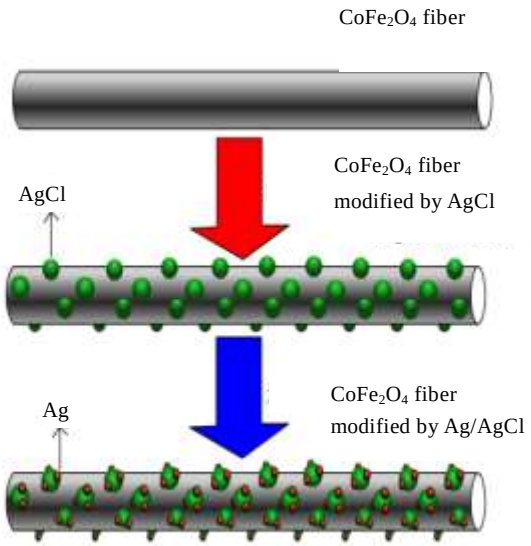

Fig.3 Schematic illustration of $CoFe_2O_4$ fiber modified by Ag/AgCl nanoparticles

Then, PVP molecule induces the nucleation and crystallization of AgCl nanoparticles in the solution and the AgCl nanoparticles are in-situ formed and attach on the surface of $CoFe_2O_4$ fiber. Subsequently, AgCl nanoparticles onto $CoFe_2O_4$ fiber are partially reduced to metallic Ag to form Ag/AgCl nanoparticles under the irradiation of UV light.

The photocatalytic activities of the as-prepared Ag/AgCl@$CoFe_2O_4$ fibers were examined by the degradation of MO in aqueous solution under visible light irradiation, and the results are shown in Fig.4. The suspension was magnetically stirred for 60 min in the dark to achieve the adsorption equilibrium of the MO on the photocatalyst powder before illumination. Control experiments in the absence of visible light irradiation indicate that AAC sample has lower capacity towards the adsorption of MO (about 6% after 60 min). The direct photolysis of MO in the absence of photocatalyst is negligible within the test period. In the presence of AAC photocatalyst and light, the degradation ratio of MO increases with the increasing irradiation time. Moreover,

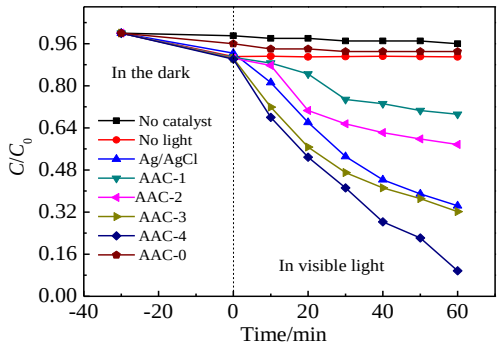

Fig.4 Degradation curves of methyl orange (MO) solution using Ag/AgCl@$CoFe_2O_4$ fibers with different packages

photocatalytic activity of AAC is gradually enhanced with the increase of Ag/AgCl loaded onto $CoFe_2O_4$ fiber. The photocatalytic activity trend follows the order: AAC-1<AAC-2<Ag/AgCl≤AAC-3<AAC-4. The content of Ag/AgCl in AAC-3 and AAC-4 sample is obviously lower than that of pure Ag/AgCl and the photocatalysis efficiency of AAC-3 and AAC-4 sample is higher than that of pure Ag/AgCl, indicating Ag/AgCl immobilized onto $CoFe_2O_4$ fiber shows higher photocatalytic activity. It is also reported that $CoFe_2O_4$ can be used as photocatalyst for the degradation of pollutant[18]. However, in our work, the as-prepared $CoFe_2O_4$ fiber (AAC-0) do not reveal any clear photocatalytic activity under the illumination of visible light and the minor reduction of MO in solution can be ascribed to the adsorption. Therefore, the species of Ag/AgCl in the composite are proved to be responsible for the degradation of MO.

Fig.5 shows the variation of UV–vis absorption spectrum of MO degradation. The maximum absorption band MO dye is located at 463 nm. The intensity of the absorption peak gradually decreases with the time increasing. Simultaneously, it is obviously observed that the maximum absorption peak of MO is red-shifted, which is attributed to the step-by-step hydroxylation process[19]. 98.2% of MO is mineralized after irradiation for 60 min, indicating MO can be degraded by AAC-4 photocatalyst under visible light irradiation.

To test the stability of photocatalyst, AAC-4 photocatalyst was collected after photodegradation experiments of MO. As shown in Fig.6a, the degradation rate becomes lower with the increasing number of recycle. However, AAC-4 still maintains 75% degradation rate after five recycles for MO, indicating the good photocatalytic stability. After every cycle, AAC-4 can be magnetically separated from the solution by a magnet as demonstrated by Fig.6b.

A series of comparative tests were further conducted to determine the reactive active species generated during the irradiation of AAC-4 photocatalyst. During the experiments, EDTA was used as holes radical scavenger and methanol or $NaHCO_3$ as hydroxyl radical scavenger. As shown in Fig.7, the addition of EDTA significantly reduces the photocatalytic activity of AAC-4 photocatalyst and only 15% of MO can be degradated. However, it can be observed that methanol and $NaHCO_3$ have a relatively little influence for photocatalytic activity, and about 65% and 60% of MO have been degradated in 50 min. These results indicate that hydroxyl (HO.) specie participates in the photocatalytic mechanism but it is not the major oxidation species in the process due to the higher reduction of the photodegradation rate when a hole scavenger is added. Photogenerated holes (h^+) on the catalyst surface must be the major active species participating in the degradation process.

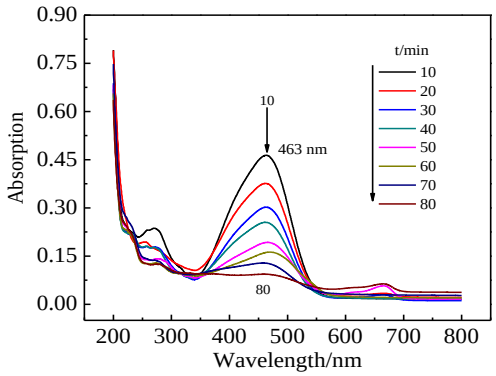

Fig.5 Time-dependent UV–vis absorption spectra of MO solution in the presence of AAC-4 photocatalyst

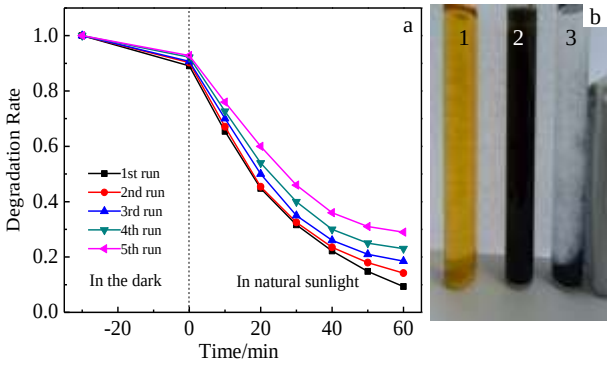

Fig.6 Photodegradation performance of AAC-4 composite over five consecutive cycles (a); magnetic separation photo of photocatalyst (1-MO solution; 2-mixture of MO and photocatalyst in solution; 3-separation of photocatalyst from the MO solution after degradation) (b)

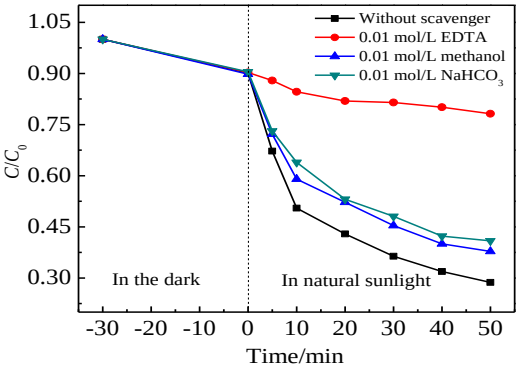

Fig.7 Effect of scavengers on degradation of methyl orange by Ag/AgCl@$CoFe_2O_4$ fiber

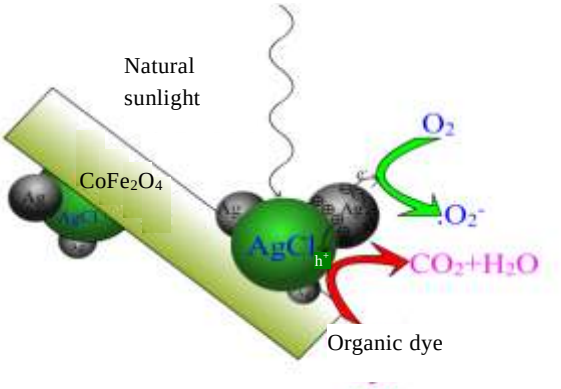

Fig.8 Schematic illustration of the photocatalytic degradation mechanism of organic dyes using the AAC crystals under natural light irradiation

Based on the above results, the photocatalytic degradation mechanism of MO using the AAC crystals under natural light irradiation can be deduced as Fig.8. Under natural light irradiation, the metallic Ag of the Ag@AgCl composite produces photogenerated electron-holes. The electrons move to the Ag nanoparticles, whereas holes move to the AgCl. The generated electrons are prevented from being transferred to Ag^+ in AgCl[20], but are instead transferred to molecular oxygen to form active species such as superoxide[21]. At the same time, the holes generated could also oxidize water to produce hydroxyl radicals, or directly oxidize Cl^- ions into Cl_0[22]. The oxidized species may interact with dye molecular to degrade into CO_2 and H_2O. In addition, well-dispersed Ag/AgCl nanoparticles onto the surface of $CoFe_2O_4$ fiber (AAC-4) possess more active sites and show higher photocatalytic activity than pure Ag/AgCl.

3 Conclusion

1) The as-synthesized AAC-4 fiber exhibits high efficiency for catalyzing the decomposition of the MO dye under visible light illumination as well as high stability and recyclability.

2) The enhancement of photocatalytic efficiency can be ascribed to the immobilization of Ag/AgCl nanoparticles onto $CoFe_2O_4$ fiber, and more active sites can be employed for the photocatalytic degradation.

3) The photocatalyst can be recycled from solution by magnetical separation due to the magnetic property of $CoFe_2O_4$ fiber. Therefore, the as-prepared AAC-4 materials with high photocatalytic activity could be promising to eliminate the dye pollutant from waste water.

References

1 Oladipo A A, Gazi M, Yilmaz E. *Chemical Engineering Research and Design*[J], 2015, 104: 264
2 Kumar V, Gohain M, Som S *et al. Physica B: Condensed Matter*[J], 2016, 480: 36
3 Volikov A B, Ponomarenko S A, Konstantinov A I *et al. Chemosphere*[J], 2016, 145: 83
4 Yagub M T, Sen T K, Afroze S *et al. Advanced Colloid Interface Scence*[J], 2014, 209: 172
5 Chen F J, Cao Y L, Jia D Z *et al. Dyes and Pigments*[J], 2015, 120: 8
6 Chowdhury S, Balasubramanian R. *Applied Catalysis B: Environmental*[J], 2014, 160-161: 307
7 Duta A, Visa M. *Journal of Photochemistry and Photobiology A: Chemistry*[J], 2015, 306: 21
8 Qamar M, Gondal M A, Hayat K *et al. Journal of Hazardous Material*[J], 2009, 170(2-3): 584
9 Vaiano V, Sacco O, Sannino D *et al. Applied Catalysis B: Environmental*[J], 2015, 170-171: 153
10 Li W, Ma Z Y, Bai G Q *et al. Applied Catalysis B: Environmental*[J], 2015, 174-175: 43
11 McEvoy J G, Cui W Q, Zhang Z S. *Applied Catalysis B: Environmental*[J], 2014, 144: 702
12 Lu L, Li J, Yu J *et al. Chemical Engineering Journal*[J], 2016, 283: 524
13 Mahmoodi N M. *Journal of Industrial and Engineering Chemistry*[J], 2015, 27: 251
14 Hosseinzadeh H, Mohammadi S. *Carbohydrate Polymers*[J], 2015, 134: 213
15 Jia Z G, Ren D P, Zhu R S. *Materials Letters*[J], 2012, 66(1): 128
16 Yu L Q, Zhang Y P, Zhi Q Q *et al. Sensors and Actuators B: Chemical*[J], 2015, 211: 111
17 Chen D L, Liu M N, Chen Q Q *et al. Applied Catalysis B: Environmental*[J], 2014, 144: 394
18 Zhang D F, Pu X P, Gao Y Y *et al. Materials Letters*[J], 2013, 113: 179
19 Lam S M, Sin J C, Abdullah A Z *et al. Separation and*

Purification Technology[J], 2014, 132: 378
20 Zhou Z D, Peng X W, Zhong L X *et al. Carbohydrate Polymers*[J], 2016, 136: 322
21 Daupor H, Wongnawa S. *Appl Catal A: Gen*[J], 2014, 473: 59
22 Wang P, Ming T S, Wang G H *et al. Journal of Molecular Catalysis A: Chemical*[J], 2014, 381: 114

铁酸钴纤维负载银/氯化银纳米粒子的合成及其对甲基橙的光催化降解

李紫宇，贾志刚，李雯雯，刘建红，江　姗，李圣标，诸荣孙
(安徽工业大学，安徽 马鞍山 243002)

摘　要：通过温和的湿化学合成法将Ag/AgCl纳米粒子固载于$CoFe_2O_4$纤维表面，固载银/氯化银纳米粒子的量可控。利用X射线衍射，扫描电子显微镜和电子显微镜等技术对制备的Ag/AgCl@$CoFe_2O_4$组成、形貌等进行了表征。以甲基橙的降解脱色为模型反应，考察了Ag/AgCl纳米粒子的不同负载量对催化性能的影响。实验结果表明：AAC-4型固载纤维光催化剂展示出比其它类型固载光催化剂以及单纯Ag/AgCl纳米粒子更高的光催化性能，可使甲基橙溶液60 min的脱色率达98.2%，且Ag/AgCl纳米粒子在$CoFe_2O_4$纤维表面的固载促进了光催化剂催化效率和催化稳定性的提升。

关键词：固载；光催化活性；甲基橙；降解

作者简介：李紫宇，男，1992 年生，硕士，安徽工业大学化学与化工学院，安徽 马鞍山 243002，电话：0555-2311807，E-mail: zjchemyue@126.com